JOURNAL OF PROPULSION AND POWER
Vol. 18, No. 4, July–August 2002

Flourescence and Temperature Measurements in an Actively Forced Swirl-Stabilized Spray Combustor

V. Santhanam,* F. C. Knopf,† S. Acharya,‡ and E. Gutmark§
Louisiana State University, Baton Rouge, Louisiana 70803

The effect of synchronized liquid fuel injection into combustion zones within excited air vortices in a small-scale model of a swirl-stabilized combustor was studied using planar laser induced fluorescence (PLIF) imaging of OH. Both the liquid fuel stream and airstream were forced at a normalized frequency of approximately 6. Air vortices were produced by acoustically forcing the airstream. The liquid fuel was modulated at the same frequency and injected at different phase angles relative to the air vortex formation. Air was forced at two levels, and both nonswirling and swirling flow situations (swirl number of 0.3) were considered. Instantaneous and phase-averaged PLIF images of OH and time-averaged temperature measurements were obtained for different phase differences between the two forcing signals. The PLIF images indicated that with forcing there was an increase in the radial distribution of the reaction zones and a decrease in the height of the flame above the nozzle exit for both nonswirling and swirling conditions. Swirl also produced better mixing along the radial direction for low forcing amplitudes. The phase difference between the two forcing signals produced a significant change in the reaction zones particularly at a low-forcing level and with swirl. The single-shot and phase-averaged PLIF images indicated that in the unforced swirling flow, high OH concentrations were obtained in two regions: an inner brush flame region and an outer flame-sheet-type region. The effect of the outer shear layer on combustion was enhanced by swirl, as the swirl increased the droplet dispersion away from the axis. With forcing, the mixing between the inner and outer regions is enhanced, and the time-averaged OH concentrations show that the primary combustion occurs in the inner core region of the flame.

Nomenclature

D	=	diameter of the exit nozzle
N_s	=	swirl number
r	=	radial distance
T	=	temperature
U	=	streamwise velocity
U_{av}	=	time-averaged streamwise velocity
U_0	=	averaged velocity at nozzle exit
x	=	streamwise distance

Introduction

THE effectiveness of any combustion system depends on the ability to maintain a stable flame at high combustion efficiencies. These are dependent on the flow characteristics inside the combustor and the degree of mixing obtained between the injected fuel and air. The mixing process in a turbulent diffusion flame involves large-scale structures, as well as small scale eddies. The dynamics of the large-scale structures play an important role in controlling the combustion and heat release process. In gaseous flames, active forcing techniques have been used to augment the role of these large-scale structures, and a number of investigators have reported that forcing leads to improved flame stabilization and higher temperatures,[1,2] improved fuel efficiency,[3] and lower levels of pollutants.[4] However, in spray flames, the mixing process is more complicated, and the interaction between the droplets and the large-scale structures are influenced by the drag force on the droplets, vaporization rate, and droplet–droplet interactions. Therefore, there is a great deal of interest in determining the nature of the large-scale structures and how they interact with the fuel droplets in spray combustors.[1,5–10] The nature of this interaction and how it is influenced by external forcing of the fuel stream and airstream is of particular interest because they provide guidance for optimizing the combustor performance and for feedback loop control.

Active forcing involves the modulation of fuel streams and airstreams at the acoustic resonant frequency of the system. The acoustic modulation of the primary airstream strengthens the coherent vortices in the flowfield. The injection of fuel droplets at the beginning of the vortex rollup (in-phase forcing) was seen to provide better mixing between the fuel droplets and airstream by cold-flow visualization.[7,10] The injection of fuel droplets after the formation of the vortices (out-of-phase forcing) was seen to produce poor mixing. This was because with in-phase forcing the droplets are entrapped in the vortices, whereas out-of-phase forcing injects them into the braid regions connecting the vortices. However, these observations are based on cold-flow visualizations and may not apply in their entirety to reacting spray flow situations.

In spray combustion systems, high temperatures affect the precombustion process by accelerating the vaporization process, thus causing the drag to drop continuously.[11] When the liquid fuel is injected from the center of the jet into its periphery, as is the case discussed in the present paper, a significant reduction of the droplet size and the drag on the fuel droplets injected along the center is, therefore, expected, and this will reduce the penetration of the droplets into the external jet shear layer. The experiments in this paper support this expectation, as will be shown later. Therefore, most of the vaporized fuel will remain in the central region of the jet. This leads to an inner shear layer between the evaporating fuel droplets in the center and the primary airstream, and the bulk of the reaction occurs in the inner shear layer. Such behavior diminishes the role of the coherent structures formed along the periphery of the primary jet. The primary goal of this study is to identify the interaction between the fuel droplets undergoing combustion and the flow structures in the primary airstream and how this interaction is affected by external forcing.

Received 12 February 2000; revision received 10 July 2001; accepted for publication 1 October 2001.

*Graduate Student, Chemical Engineering Department.
†Professor, Chemical Engineering Department.
‡Professor, Mechanical Engineering Department.
§Professor, Mechanical Engineering Department, Univ. of Cincinnati.

As noted earlier, forcing is expected to increase fuel–air mixing, which can have several potential benefits including increased fuel efficiency, greater heat release and more compact combustion, more uniform temperature distributions, and lower emissions. All of these benefits are potentially advantageous for a gas turbine combustor. In the present work, the focus has been to look at heat release and combustion (as indicated by the OH emission) and to explore forcing techniques to enhance this measure or metric. By looking at the spatial distributions of the OH images, we have also made conclusions about the uniformity of the heat release and temperature distributions.

OH planar laser-induced fluorescence (PLIF) images are an important diagnostic tool used in the characterization of reaction zones in flames.[12–15] Instantaneous and phase-averaged OH PLIF images have been used to study the rollup and growth of these large-scale structures in gaseous flames[16] and in liquid fuel combustion.[17–19] In the present paper, the majority of the results presented and the associated analysis is based on OH PLIF images collected.

Experiments

The tests were performed using a small-scale model of a swirl-stabilized combustor operating at nearly 30-kW heat release (Fig. 1) assuming stoichometric combustion. This assumption is based on the fact that all measurements are made without confining the flame and that there is significant entrainment of air from the surroundings. The combustor had a single unheated primary airstream, which could be acoustically modulated and swirled. At the center of the air jet, liquid fuel, ethanol, was injected through an atomizer fogger in a conical pattern using an automotive fuel injector that could be pulsed using a signal generator.

A schematic of the combustor and control block diagrams of the system are shown in Figs. 1 and 2. Axial and swirling airstreams were issued from a circular chamber through a conical nozzle with a 3.8-cm exit diameter. The chamber was utilized both as an acoustic resonator and a settling chamber. It contained a honeycomb to straighten the flow and two acoustic drivers to apply acoustic excitation to the jet. The tests were performed with total airflow rate of 85 l/min. The swirl was applied aerodynamically, with tangential air injection upstream of the nozzle exit. Changing the momentum ratio between the axial flow and the tangential jets varied the swirl number. The maximum swirl number tested was $N_s = 0.30$. The swirl number was computed using constant-temperature anemometer measurements of the axial and tangential velocity components at the jet exit.

Fuel was injected through a 0.3175-cm tube mounted in the center of the air nozzle. A pressure fed fogger (manufactured by Arizona Mist, Inc.), which was mounted upstream of the nozzle exit, was used to atomize the ethanol fuel. The fogger consisted of a swirl chamber with a 0.3-mm-diam exit orifice. Droplet sizes produced had a Sauter mean diameter of around 40 μm. Injector pressures were typically in the range of 80 psig. The fogger produced a full-cone spray with the smaller droplets (less than 30 μm) concentrated in the central regions.[8] As noted, the atomized liquid fuel was pulsed using an automotive fuel injector. The fogger location could be adjusted between 1 and 2 cm upstream of the combustor nozzle. Preliminary testing showed the optimal fogger location to be approximately 1.9 cm upstream of the nozzle exit. The optimal location was based on a visual inspection of the flame and its stability for different fogger locations.

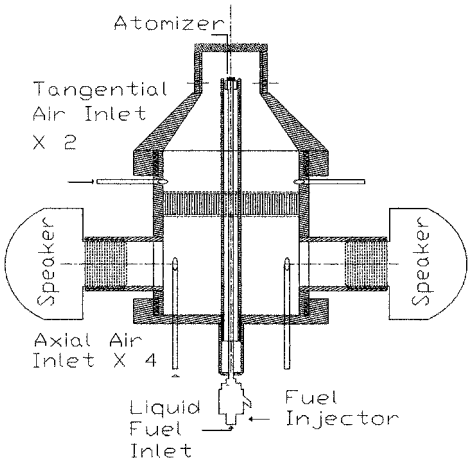

Fig. 1 Swirl-stabilized spray combustor.

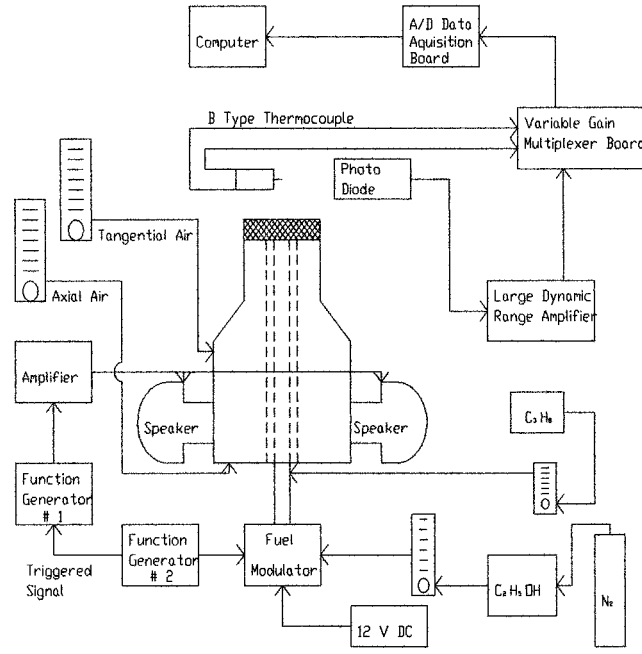

Fig. 2 Control block diagram of experimental setup.

To study the interaction between the jet vortices and the fuel droplets, the jet was acoustically excited at the acoustic resonance frequency of the settling chamber. Measurements of maximum pressure and velocity fluctuations found this resonant frequency to be 200 Hz, corresponding to the Helmholtz resonance (see Stephens et al.[7]). The fuel was subsequently injected into the vortices at the same modulation frequency as air with a duty cycle of 50% (the valve is open during one-half of the cycle). The response of the fuel injection system was verified using high-speed video recording of images captured by using triggered stroboscopic light flashes. Temperature measurements over a wide range of frequencies showed a maximum heat release when operating at the resonant Helmholtz frequency due to enhanced entrainment and mixing in the vortices induced by forcing.[1,5,6]

The phase between air and fuel pulsing could be varied in the experiments through the full range of 360 deg. When the relative phase or timing of the fuel injection was varied with respect to the vortex formation cycle, different mixing patterns could be achieved. A goal of this work was to evaluate the effect of the phases on the combustion behavior.

Optical Diagnostic System

The excitation system used for the PLIF measurements consisted of a dye laser pumped by a Nd:YAG laser. The dye laser output was frequency doubled using a BBO I crystal to provide appropriate UV radiation. The YAG laser pumped at about 240 mJ/pulse with a frequency of 10 Hz at 532 nm. The dye laser used rhodamine 6G to produce light at about 567 nm with an energy of ~60 mJ/pulse. This was then frequency doubled to give light at 283.4 nm with an energy of ~6 mJ/pulse. This was then spread into a sheet of about 10 cm high and 0.03 cm wide, having a pulse duration of 20 ns using cylindrical lenses. The frequency-doubled light was tuned to specific rovibronic transitions of the (1,0) band of OH using the off-resonance excitation/detection strategies described by Allen et al.[18]

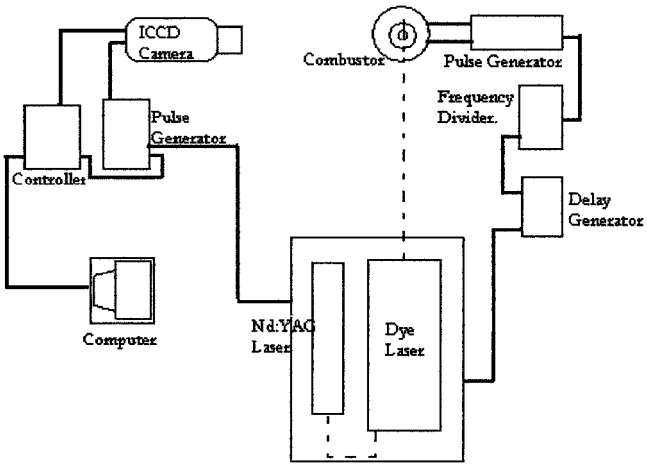

Fig. 3 Schematic of experimental setup.

The PLIF images were obtained by collecting the fluorescence orthogonal to the incident laser sheet using a 105 mm, ƒ/4.5 UV telephotographic lens attached to a intensified and cooled charge-coupled device (CCD) camera having a format of 384 × 576 pixels. The field of view of the camera was 13.3 cm vertical by 20 cm horizontal. The intensifier was triggered synchronously with the laser pulse and was gated for a duration of 10 ns. The signal-to-noiseratio was increased by using a mechanical shutter with period of 1 ms, in preopen mode, in front of the camera. This also prevented blooming due to phosphorescence persistence in the camera. A 10-nm narrow-bandpass interference filter centered at 315 nm was used to effectively collect OH fluorescence from the (1,1) band.[20] This effectively discriminated against elastically scattered laser light for most of the cases.

A schematic of the setup used for obtaining phase averaged PLIF images is shown in Fig. 3. The relay network between the air-forcing signal and the laser trigger consists of a frequency divider to obtain pulses at 10-Hz frequency from a 200-Hz signal and a time delay to enable imaging along the forcing cycle.

The phase averaging was done for a total of 50 images taken consecutively at the same time instance (phase) during an air-forcing cycle, for different phase lags and forcing levels with and without swirl. A few cases were averaged for 200 shots but did not show any improvement in the visualization of the structures.

Results

Results for 16 different cases, as given in Table 1, are presented. The parameters varied include the forcing level, swirl number, and the phase difference between the airstream and the fuel stream modulation.

Calibration

A qualitative calibration of the OH radical concentration was made using water vapor present in atmospheric air at high temperatures as a calibration source for OH radical.[21] The calibration was performed primarily to ensure that the PLIF system was providing the right quantitative estimates of the OH concentration. For this purpose, the experimentally determined OH values were compared with theoretical values. This calibration neglects the effects due to variation in quenching cross section across the flame and also the variation in intensity across the laser sheet. The calibration curve corresponding to the unexpanded sheet is shown in Fig 4. The measured fluorescence intensity is normalized to the theoretical OH mole fraction at the highest temperature attainable in the furnace, and the other values are estimated from this. This is then scaled to the expanded sheet. The theoretical calculations for the disassociation of water vapor are well known and were performed using GASEQ©.¶ The measured humidity along with the atmospheric mole fractions of N_2 and O_2 was prescribed as the initial composition. The following species were included in the chemical equilibrium calculation: H, N, O, H_2, N_2, O_2, H_2O, OH, H_2O_2, NO, and NO_2. As seen in Fig. 4, the experimental and theoretical values fall right on top of each other, providing confidence on the OH values measured by the PLIF system.

¶GASEQ is a chemical equilibrium program for Windows by C. Morley. Data available online at http://dspace.dial.pipex.com/c.morley/.

Table 1 Conditions for the 16 different experimental runs

Case	Forcing	Swirl no.	Phase lag	Case	Forcing	Swirl no.	Phase lag
1	Low	0	0	9	High	0	0
2	Low	0	90	10	High	0	90
3	Low	0	180	11	High	0	180
4	Low	0	270	12	High	0	270
5	Low	0.3	0	13	High	0.3	0
6	Low	0.3	90	14	High	0.3	90
7	Low	0.3	180	15	High	0.3	180
8	Low	0.3	270	16	High	0.3	270

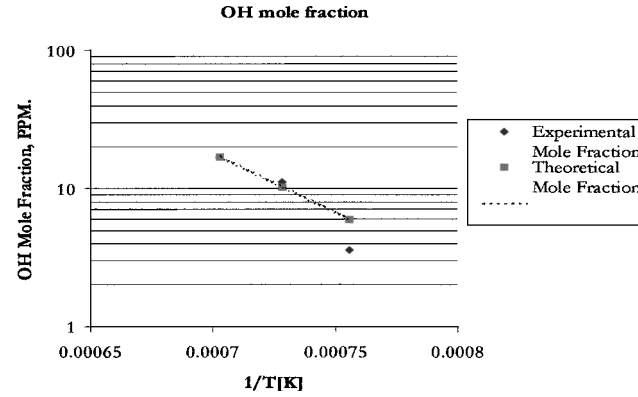

Fig. 4 Calibration of OH mole fraction.

Flow Measurements

Detailed flow measurements for the flow conditions reported have been made by Stephens[8] and have been reported by Stephens et al.,[7] Stephens,[8] and Stephens et al.[9] Figure 5 shows the smoke visualization pictures of the nonreacting gaseous flowfield (no spray injected) with high-level forcing. Similar images were also obtained with the low-level forcing case, although the sizes of the structures were slightly different. These images were taken by seeding the air with smoke and using a CCD camera triggered at different instances of the forcing cycle. The evolution of vortical structures at four instances during the forcing cycle is clearly seen in Fig. 5. The structures are axisymmetric and have dimensions comparable to the jet diameter. Only the first two structures can be seen clearly because farther downstream, the smoke has dispersed considerably to enable clear imaging of these structures. Because fuel droplets are injected at the geometric center of the airstream, it is anticipated that these droplets will be entrained by the vortical structures. Thus, the timing of the fuel injection relative to the vortex evolution is likely to play an important role in the combustion process.

Figure 6 shows the mean centerline velocity distribution plotted as a function of the axial distance for both the forced and unforced cases. These measurements were again made for the nonreacting gaseous flow (under replicate inflow conditions as the reacting flow) with a hot-wire anemometer using a single-wire probe and were later confirmed with laser Doppler velocimeter measurements. Results are presented for both swirling and nonswirling flows. For nonswirling flows, a slight increase in velocity followed by a potential core region is observed until $x/D = 3$. Beyond $x/D = 3$, the centerline velocity decays due to jet spreading and entrainment of surrounding air. With forcing, the centerline velocity accelerates rapidly downstream of the nozzle until about $x/D = 1.8$ due to acoustic streaming of the flow. Beyond $x/D = 1.8$, the centerline velocity decays, with the decay rate considerably larger than the unforced case. Thus, forcing induces greater spreading of the jet and

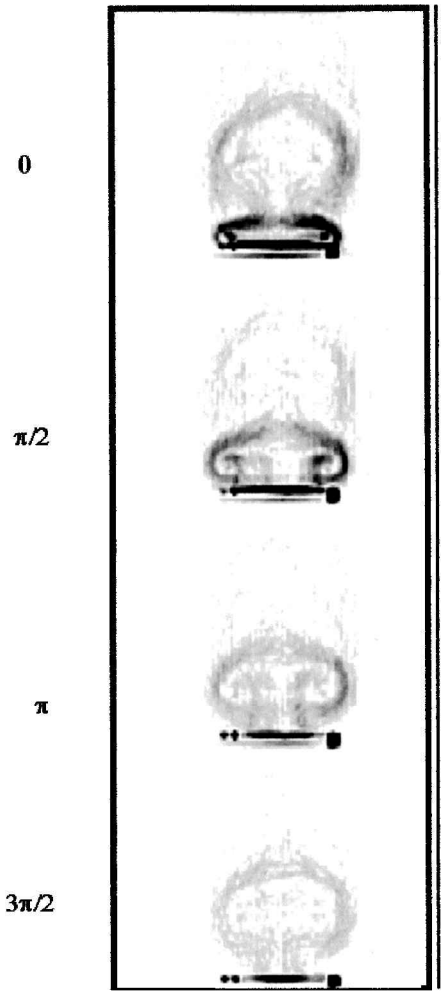

Fig. 5 Smoke visualization of nonreacting flow with forcing; numbers denote different time instances during the forcing cycle.

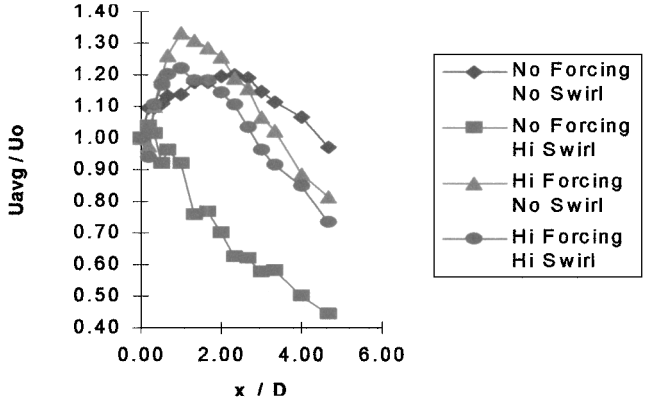

Fig. 6 Mean velocity for the unforced and forced cases.

increased entrainment from the surroundings, leading to the more rapid decay observed in the centerline velocity. For the swirling flow, the centerline velocity exhibits a different behavior with the velocity decaying immediately downstream of the centerline. Note that at the low swirl numbers investigated (0.30), although a velocity defect is generated, a central recirculation leading to negative velocities is not produced. With forcing, the centerline velocity profile is similar to that without swirl, indicating that forcing exhibits control authority even in the presence of swirl.

The centerline turbulence intensity at the nozzle exit, $x/D = 0$, was approximately 15%. With forcing, a flow oscillation was superimposed, and low and high forcing corresponded to two levels of normalized velocity fluctuations (which include the effect of the

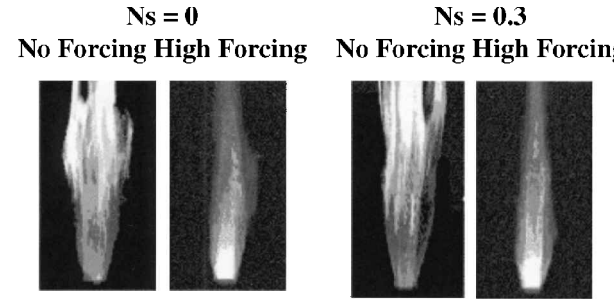

Fig. 7a Flame images.

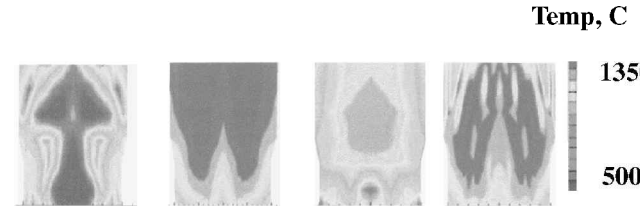

Fig. 7b Temperature contours.

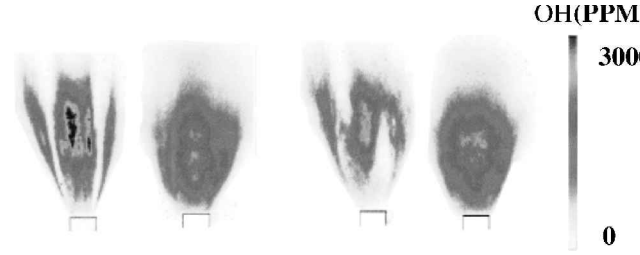

Fig. 7c Time-averaged PLIF images of OH.

forcing oscillations) at the jet exit (u'/U_0), with rms values of 30 and 60%, respectively.

Temperature and Time-Averaged OH Plots

The temperature contours measured with a type B thermocouple (compensated for radiation effects) along with the corresponding time-averaged PLIF images and video images are shown in Fig. 7 for four cases. These cases included the unforced and forced nonswirling flames and unforced and forced swirling flames at a swirl number of 0.3. The forced cases shown are for a zero-phase difference between the fuel injection and the air forcing. Note that both fuel modulation and airstream modulation could impact the atomization process itself, which, in turn, will effect the spray combustion. However, as shown earlier in the centerline velocity plots, a dominant effect of forcing is the entrainment of air and alteration of the flow dynamics of the jet. It is this mechanism that appears to provide the primary effect. Note that the temperature measurements were made only in one-half of the flame (from the centerline outward), and these measurements are reflected to the other half, assuming symmetry.

The temperature plot for the unforced nonswirling case shows a cold core with higher temperatures along its periphery. This indicates that the significant reactions occur in the shear layer surrounding a colder core of evaporating droplets. The high-temperature regions were in a very thin band, which indicated diffusionlike combustion due to the poor radial mixing between the fuel vapors and the primary air. The flame images show large amounts of yellow radiation due to blackbody emission from soot, and the blue chemiluminescence emission from CH/C2 at the flame base was weak. Swirl increased the temperature in the central region of the jet and moved the location of heat release closer to the jet exit. The high-temperature region was also wider. The amount of yellow emissions was somewhat reduced, and the blue chemiluminescence was enhanced and shifted upstream. Forcing of the airstream had a

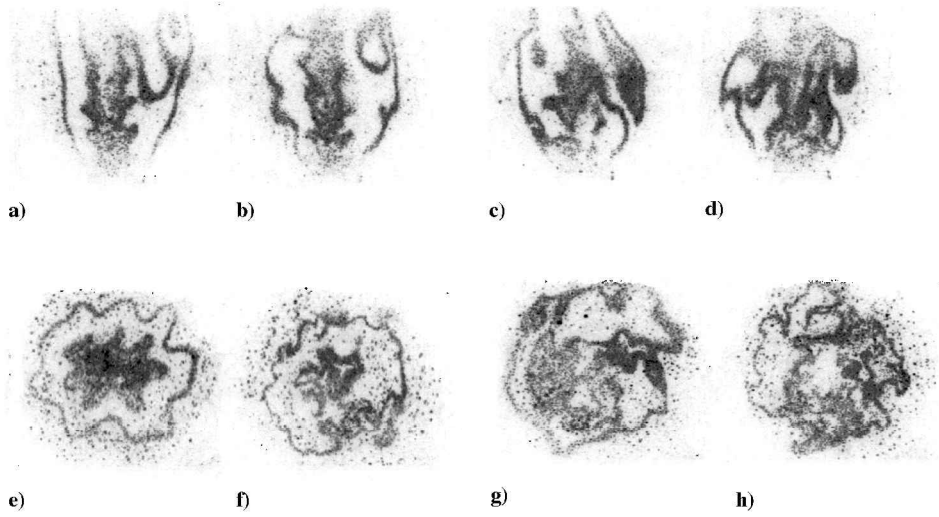

Fig. 8 Instantaneous PLIF images, longitudinal midplane slices: a) $N_s = 0$, unforced; b) $N_s = 0$, forced; c) $N_s = 0.3$, unforced; d) $N_s = 0.3$, forced, and horizontal plane slices at $x/D = 0.53$; e) $N_s = 0$, unforced; f) $N_s = 0$, forced; g) $N_s = 0.3$, unforced; and h) $N_s = 0.3$, forced.

strong effect on the appearance of the flame in both nonswirling and swirling flames. The yellow emission was eliminated, and the intensity of blue chemiluminescence at the flame's base was significantly increased. This effect was also recorded in the temperature measurements. The temperatures in a large area at the flame center near the jet exit increased considerably, thus contributing to better stabilization of the combustion process. The forced nonswirling flame exhibited slightly higher temperature compared to the forced swirling flame. High temperatures covered a larger area both radially and axially. The forced flame was more compact, possibly due to the accelerated cooling by the large quantities of ambient air, which was entrained into the flame by the vortices and intensely mixed. The high-temperature region near the flame base extended in the radial direction more from the swirling flame than the nonswirling flame due to the increased radial dispersion of the fuel droplets by the centrifugal forces. Thus, it is seen from the temperature contour plots that both forcing and swirl lead to increased heat release and more stable combustion.

The trends observed from the temperature contour plots were confirmed in the time-averaged PLIF images (Fig. 7c). Each of these images represent an area of 12 cm high and 11 cm wide. The location of the nozzle is shown by a solid black line at the bottom of the image. The regions with the highest intensity of OH fluorescence are only qualitatively indicative of the approximate location of the reaction zones. This is because OH can be convected to post-flame regions without being quenched. In the baseline unforced nonswirling case, two distinct reaction regions can be discerned: an inner zone and a thin circumferential region. The two regions are separated by inactive zone of the high-speed and low-temperature annular jet. Within the internal region, one can distinguish very dark regions, which were caused by Mie scattering from atomized fuel droplets before complete vaporization. This conclusion was based on the observation that only for the baseline unforced case droplets were seen escaping the flame region. The fuel droplets lead to lowering of the temperatures in the inner region as seen in the temperature plot. High concentration of OH appeared at over one diameter downstream of the nozzle, consistent with the low temperature measured in the near field of the partially lifted flame for these conditions.

Swirl increased the mixing rate between the external shear layer and the jet center. The reaction zone was concentrated in the central area as observed earlier from the temperature measurements. The flame was still partially lifted, but the stronger dispersion of the droplets by the swirling motion eliminated the Mie scattering interference observed in the baseline case. Addition of forcing shifted the reaction zones upstream toward the nozzle and intensified the production of OH radicals in this area. This helped in stabilizing the flame. The external and internal reaction zones merged due to the intense mixing action of the vortices. Forcing was as effective in increasing the flame temperatures with swirl as for the nonswirling case.

Single-Shot PLIF Imaging

Single-shot OH images of the four cases discussed in the preceding section are shown in Fig. 8. Both longitudinal cuts and cross-sectional cuts are show. The longitudinal images were taken on a plane including the flame's axis, and the cross-sectional images were taken at a plane perpendicular to the axis at an axial distance of $x/D = 0.53$ from the nozzle.

The longitudinal slice in the unforced case (Fig. 8a) is comparable with those obtained for a heptane–air spray flame studied by Allen et al.[18] An important feature of the no-swirl case is the presence of two concentric reaction zones, which indicates the presence of a mixing layer between the pulsed vaporizing fuel jet and the primary air and another shear layer between the primary air and the surrounding atmosphere. The horizontal slices exhibited azimuthal symmetry, and the wavy nature of these reaction zones indicate that there are three-dimensional effects present in these shear layers. Both internal and external reaction zones exhibit an azimuthal wrinkling of the flame with 7–8 circumferential cycles. In the swirling case, the single-shot images show strong interaction between the two zones (Fig. 8g), which is consistent with the effect of centrifugal forces imposed on the droplets by the swirling motion that tends to move them outward in the radial direction. The swirl reduced the azimuthal wave pattern observed in the baseline case. The effect of forcing was to increase the radial mixing due to increased entrainment of air from the periphery (Figs. 8b, 8d, 8f, and 8h). It is seen that forcing and swirl both tend to increase the mixing and, thus, improve combustion. The wavelength associated with the wrinkling of the forced swirling flame was smaller than all other cases (Fig. 8h). The presence of large-scale structures in the inner shear layer of the nonswirling flames (Figs. 8a and 8b), is attributable to the pulsation of the liquid fuel. Forcing of the airstream at the resonant frequency induced or reinforced some large-scale structures in the outer shear layer of both nonswirling and swirling flames (Figs. 8b and 8d). Unburned fuel droplets in the unforced case without swirl were identified as the dark spots in the center of the horizontal slice (Figs. 8a and 8e). These spots are due to the Mie scattering from relatively large unburned droplets. Their presence was also corroborated by the fuel droplets, which condensed on the thermocouple only in the case of the unforced flow.

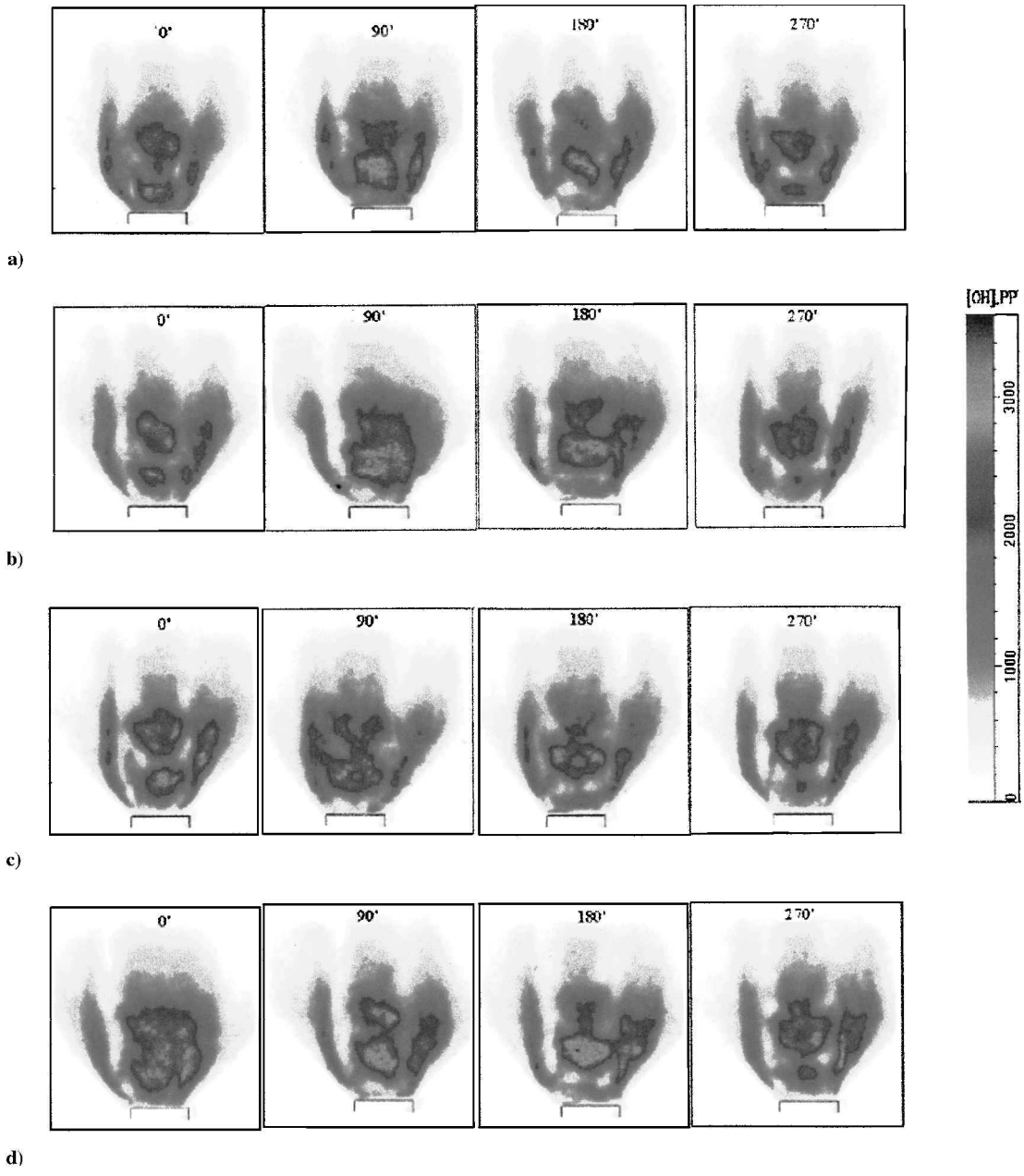

Fig. 9 Phase-averaged PLIF images for low forcing, $N_s = 0$ case: a) phase lag = 0, b) phase lag = 90, c) phase lag = 180, and d) phase lag = 270.

Phase-Averaged PLIF Imaging

Phase-averaged PLIF images were obtained for each of the 16 cases shown in Table 1 and are shown in Figs. 9–12. Each row in Figs. 9–12 represents a different phase lag between the fuel injection and the air vortex formation. The phase lag was varied 0 (in-phase injection), 90, 180, (out-of-phase injection) and 270 deg. In each row, phase-averaged images at different time instances or different phase angles during one cycle of the forcing signal of the airstream are shown.

The general trends exhibited by the phase-averaged images agree qualitatively with the temperature contours reported by Stephens et al.[7] for nearly identical conditions in the same geometry. The reaction zones are broader and more uniform with forcing and also with swirl, as indicated by the temperature contours. Qualitative comparison between OH concentration and temperature level is justified because regions with high temperatures and oxidizer concentration approximately correspond to the reaction zones. However, care should be taken in doing a direct quantitative correlation because temperature contours are proportional to the ratio of PLIF signals at two different resonant wavelengths rather than OH fluorescence at a single transition.[22] Also, OH radicals can be present not only at the reaction zones, but also in postflame hot regions.

Low Forcing, $N_S = 0$

The phase-averaged PLIF images for the no-swirl, low-forcing cases are shown in Fig. 9. Two distinct reaction zones could be discerned at the low-forcing level conditions, an internal zone near the flame centerline and an external one at the flame circumference. However, the PLIF images show that the main reaction zone with the strongest OH appears to be the internal region, which implies that a significant portion of the droplets are essentially concentrated in the inner region of the jet. Whereas the outer shear layer region represents a larger surface area, the OH levels in this region are lower. This observation is in contrast to earlier cold-flow visualizations, which indicated that the significant portion of the droplets were entrained into the annular external shear layer vortical regions.[7] These observed differences in the dispersion of the fuel droplets between the cold-flow and the reacting-flow cases confirm the earlier speculations that due to fuel vaporization the drag force is reduced when combustion is present, leading to a reduction in the interaction

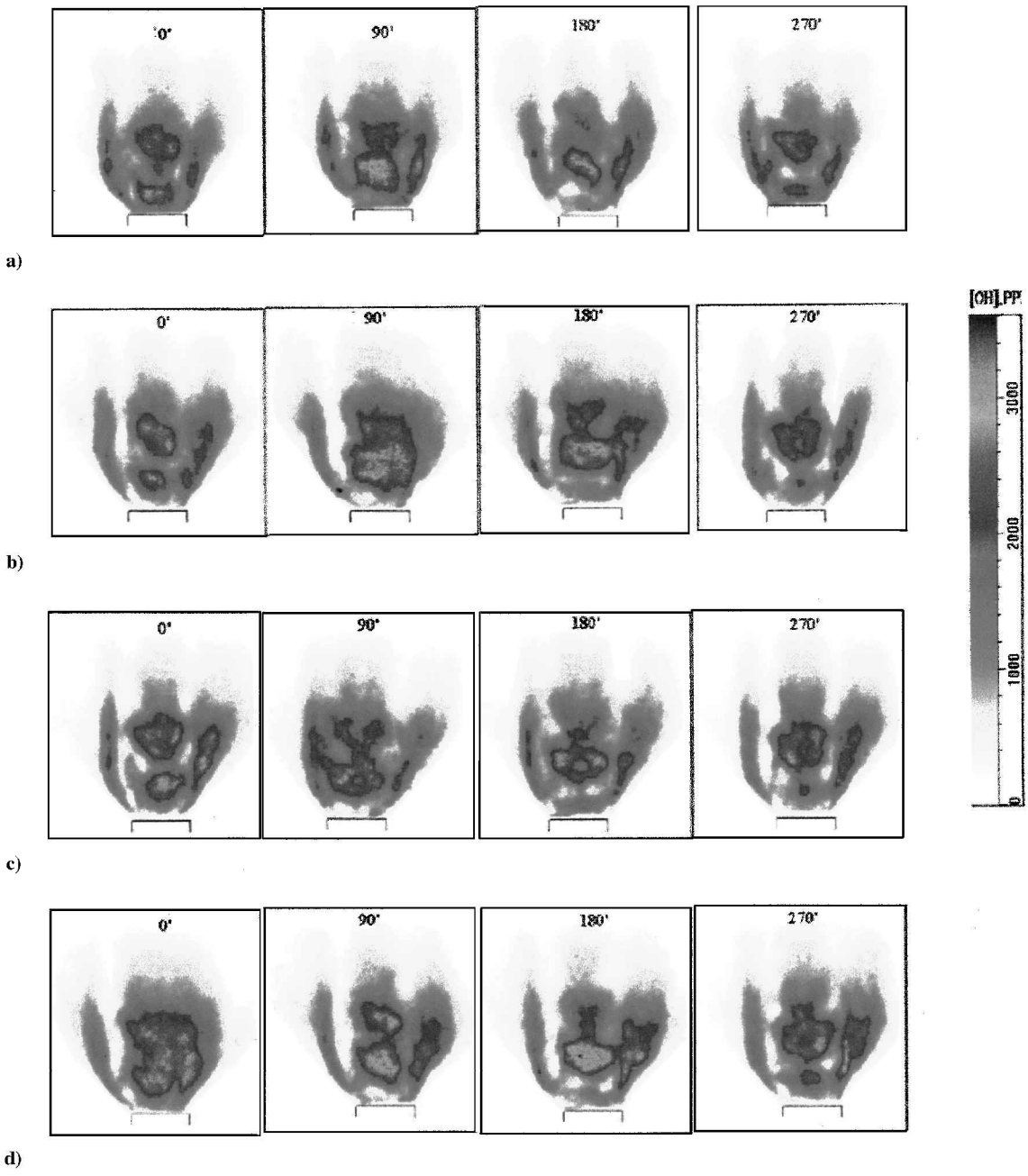

Fig. 10 Phase-averaged PLIF images for low forcing, $N_s = 0.3$ case: a) phase lag = 0, b) phase lag = 90, c) phase lag = 180, and d) phase lag = 270.

of the droplets and the external airstream. With a lower drag, the droplets are more likely to follow a path defined by their initial conditions. Furthermore, in the absence of swirl, the droplets do not experience the centrifugal force driving them radially outward, and therefore, the droplet density in the outer shear layer is expected to be lower in nonswirling flows. This also limits the interaction between the droplets (or the number of droplets) and the external airstream. Therefore, the phase difference between the fuel injection and the external airstream forcing did not produce a substantial change in the reaction zones on the periphery. Noted from the PLIF images that the reaction zones appear to be larger, due to increased combustion, at about one-half of a cycle following the completion of fuel injection. This is consistent with that the duty cycle of fuel injection is 50%, and the fuel injection is essentially completed 180 deg (half a cycle) after fuel injection is initiated

Fuel injection was begun at phase angle 0 for in-phase injection (Fig. 9a). Two reaction zones could be discerned along the axis, corresponding to fuel packets that were injected during the last and previous cycles. In some cases it was possible to follow the combustion of the fuel packets during two full cycles. The images indicated that, unlike the unforced case, combustion was initiated immediately downstream of the nozzle due to the strong air entrainment induced by the air forcing. Primary combustion was essentially completed within a distance of two diameters from the nozzle. In the absence of swirl, the amount of reaction in the external shear layer was limited because most of the fuel was consumed within the central part of the flame.

For phase lag of 90, 180, and 270 deg, the fuel injection is initiated at different instances during the air-forcing cycle, which are at 270, 180, and 90 deg, respectively. At these various degrees of out-of-phase fuel injection, the cold-flow visualizations by Stephens et al.[7] had shown that the fuel droplets were not fully entrained by the air vortices. No such observations can be identified in the images in Fig. 9. This indicates that, for reacting flows, the interaction between the droplets and the coherent structures is considerably weaker than for nonreacting flows. The OH images do, however, indicate that the spatial distribution of the reaction zone was shifted farther away from the center than for the in-phase injection.

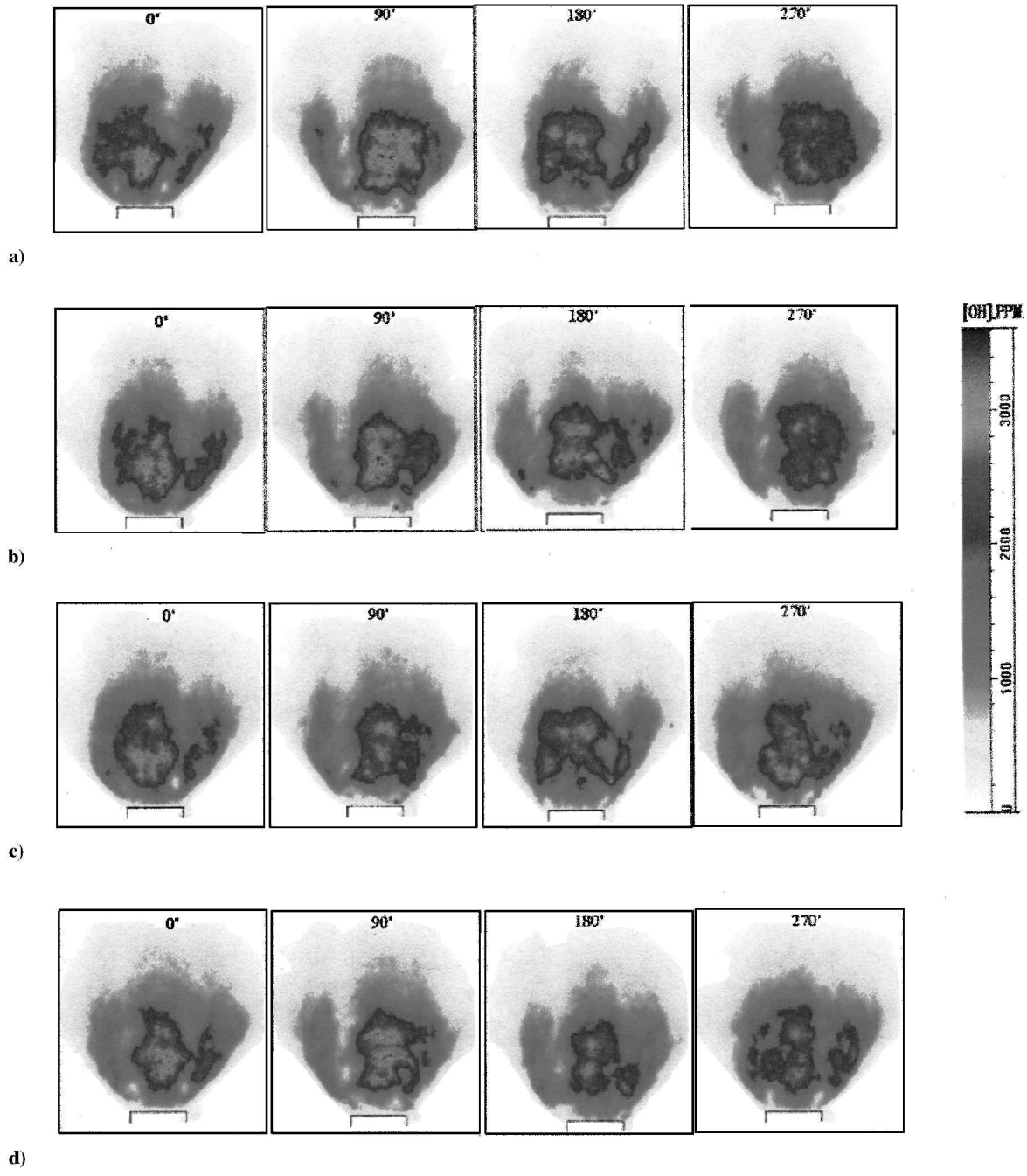

Fig. 11 Phase-averaged PLIF images for high forcing, $N_s = 0$ case: a) phase lag = 0, b) phase lag = 90, c) phase lag = 180, and d) phase lag = 270.

Low Forcing, $N_S = 0.3$

Figure 10 shows the OH images for low forcing in the presence of swirl. The addition of moderate swirl broadened the internal and external reaction zones and caused partial merging of the two zones. The swirling flow increased the mixing rate of the fuel droplets such that the images during a single cycle did not show the injection of fuel packets as clearly as in the non swirling case.

The phase lag of fuel injection in the swirling flame had a much more significant effect than in the nonswirling case. This could be due to increased radial dispersion of droplets causing the structures in the outer shear layer to play a bigger role in combustion. For the cases corresponding to phase lag of 0 and 90 deg (Figs. 10a and 10b), the reaction zones were significantly larger than for the 180 and 270 phase-lag cases (Figs. 10c and 10d).

Compared to the nonswirling case, the in-phase injection showed much stronger radial mixing. The significantly greater width of the reaction zone was due to better radial dispersion of the droplets. The amount of OH radical varied during a cycle, with a maximum at 0 deg and a minimum at 180 deg. The images for a phase lag of 90 deg showed very small variation in the amount of OH during one cycle.

The reaction zones appeared considerably smaller for out-of-phase fuel injection (Fig. 10c) indicative of poor combustion efficiency. The injection of fuel at 180 deg into the air vortex cycle can be clearly seen, and the evolution of the reaction zone during the cycle is discernible. The images for a phase lag of 270 indicated that this condition had the lowest rate of combustion.

High Forcing, $N_S = 0$

The increased forcing level resulted in a significant increase in the combustion intensity, as seen in Fig. 11. The reaction zones were larger and more uniform, and the higher levels of OH indicated efficient combustion. The images show better radial mixing than in the low-forcing case. The internal and external reaction zones were less conspicuous but were still discernable in several cases. These changes were a consequence of the strong entrainment induced by

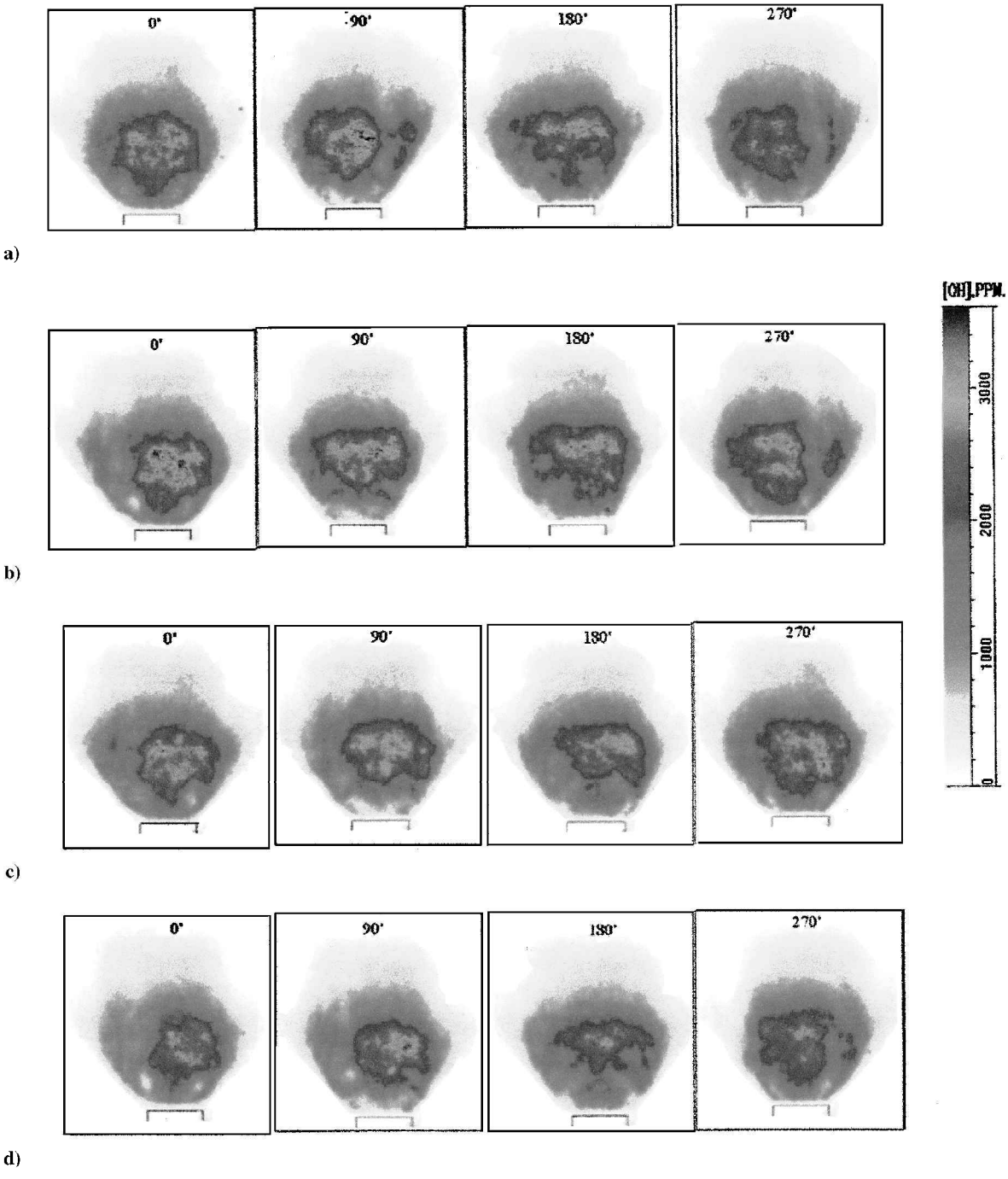

Fig. 12 Phase-averaged PLIF images for high forcing, $N_s = 0.3$ case: a) phase lag = 0, b) phase lag = 90, c) phase lag = 180, and d) phase lag = 270.

the high-forcing level, causing high radial velocities near the flame base. The radial velocity, which was directed toward the flame center, resulted in low combustion level near the exit of the nozzle and more uniform axial and radial OH concentration profiles. The intense combustion at the central region of the flame and the high temperatures resulted in rapid vaporization and low dispersion during the lifetime of the droplets. The images showed uniform reaction zones throughout the cycle, and the fuel injection cycle is not identifiable. The effect of phase lag is small compared to the low-forcing cases, although the 0- and 90-deg phase lag show slightly more heat release than the other two cases.

High Forcing, $N_s = 0.3$

Swirl combined with high forcing effectively produces the strongest combustion. The OH defined reaction zones, as shown in Fig. 12, were larger than in Figs. 9–11. Both swirl and forcing substantially enhanced the mixing between the inner and outer regions, and the presence of two independent shear layers was not identifiable. Furthermore, the variation of OH fluorescence during any of the measured cycles was very small.

The effect of fuel injection at different phase lag in the swirling cases was minimal, with lowest level of OH measured at 180 and 270 deg of phase lag.

Centerline OH Distributions

To provide quantitative assessment of the OH distribution, the centerline OH values for the case of low swirl is presented in Fig. 13. The vertical axis represents OH concentrations in parts per million, whereas the horizontal axis represents the axial distance along the centerline. The axial distance corresponding to the peak OH is considerably closer to the nozzle for the forced cases. This is consistent with the earlier PLIF images and temperature

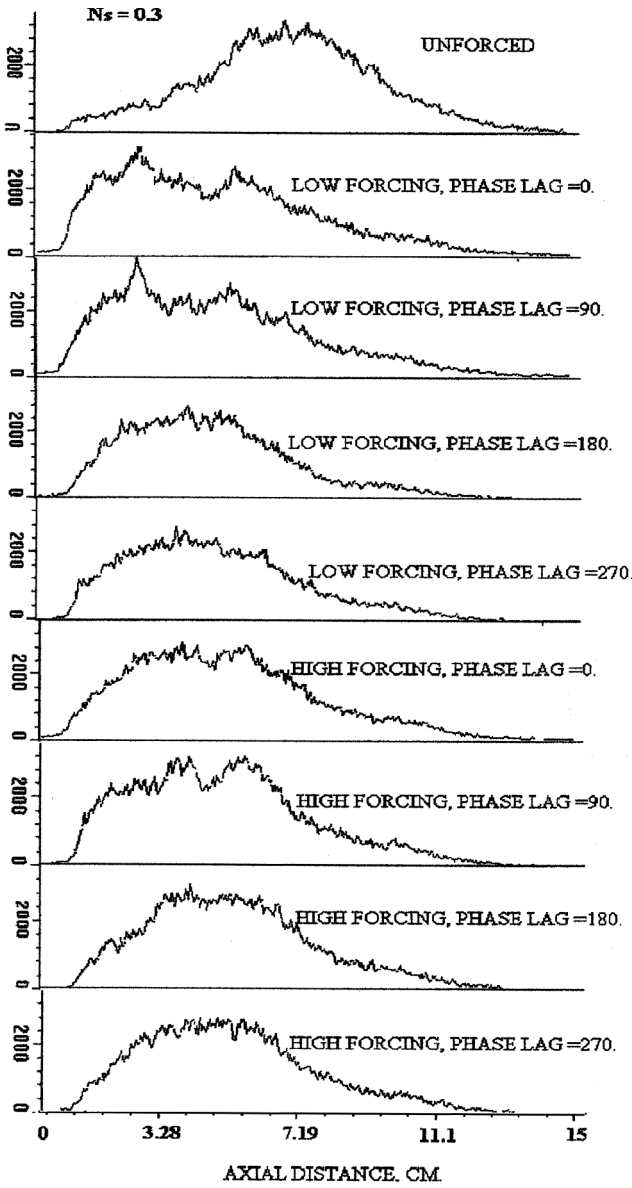

Fig. 13 Centerline distribution of OH for the swirl ($N_s = 0.3$) case.

plots. The effect of phase can be more clearly seen for the low-forcing cases, where the location of the OH peak for the 0- and 90-deg phase lag is closer to the nozzle than the corresponding location for the 180- and 270-deg phase lag. For the high-forcing cases, as noted earlier, the mixing between the inner and outer zones is quite intense, and phase lag has a marginal effect.

Conclusions

The effects of forcing and swirl on the flame structure of a swirl-stabilized spray combustor have been studied using temperature and OH PLIF measurements. Forcing had a strong influence on both nonswirling and swirling flames. The baseline flame that was unforced and with no swirl was sooty and exhibited large amounts of blackbody yellow radiation from soot particles. The temperature and OH distributions showed internal and external active reaction zones. The internal reaction zone corresponds to the evaporating fuel jet stream which entrains air, whereas the external reaction zone corresponds to the forced primary airstream. For the unforced case, the external active heat release region was limited to a narrow region at the circumference of the jet, similar to a diffusion flame. Under these conditions, poor mixing with the ambient air and low vaporization rate contributed to this behavior. Addition of moderate swirl enhanced the combustion at the base of the flame and increased the heat release near its center due to enhanced fuel dispersion and improved mixing. Forcing eliminated the yellow emission in both nonswirling and swirling flames and significantly enhanced the heat release. The flame became wider at the base and was more compact, and the two distinct reaction zones were unified. The intensified air entrainment by the large-scale vortices produced by the jet forcing enhanced the combustion rate near the jet center and accelerated the vaporization process. Most of the fuel was consumed inside the jet and, thus, the interaction with the external shear layer was minimal.

The effect of varying the phase between the fuel injection and the airstream modulation was most evident for the case of low forcing and swirl. The best conditions (largest OH regions) corresponded to the in-phase condition followed by the 90-deg phase lag conditions. Mixing and combustion was poor for both the 180- and the 270-deg phase lag conditions. At high-forcing levels, the enhanced entrainment and mixing reduces the effect of phase lag. Furthermore, the combination of forcing and swirl minimized variations of the OH PLIF concentrations (which are approximately representative of heat release variations) during one cycle and can potentially reduce the tendency of the combustion to become unstable in an enclosed combustion chamber configuration.

Acknowledgments

The work was supported by NASA/LEQSF under the EPSCoR program, and by the Propulsion Program of the Office of Naval Research. Their support is gratefully acknowledged. We would like to acknowledge Chris Morley for allowing us to use his program for theoretical calculations. Flow measurements reported in this paper were performed by Jonathan Stephens, and his efforts are acknowledged.

References

[1]Stephens, J. R., Acharya, S., Gutmark, E. J., and Allgood, D. C., "Active Forcing of Air and Fuel Feed in Swirl Stabilized Spray Combustion," *International Society for Air Breathing Engines*, 1997.

[2]Schadow, K. C., Gutmark, E., and Wilson, K. J., "Active Combustion Control in a Coaxial Dump Combustor," *Combustion Science and Technology*, Vol. 81, 1992.

[3]Gutmark, E., Parr, T. P., Hanson-Parr, D. M., and Schadow, K. C., "Use of Chemiluminescence and Neural Networks in Active Combustion Control," *Twenty-Third Symposium (International) on Combustion*, Combustion Inst., Pittsburgh, PA, 1990.

[4]Gutmark, E., Parr, T. P., Wilson, K. J., Yu, K. H., Smith, R. A., Hanson-Parr, D. M., and Schadow, K. C., "Compact Waste Incinerator Based on Vortex Combustion," *Combustion Science and Technology*, Vol. 121, 1996.

[5]Stephens, J. R., Acharya, S., and Gutmark, E. J., "Swirl-Stabilized Spray Combustion with Periodic Heat Addition," AIAA Paper 97-0464, Jan. 1997.

[6]Stephens, J. R., Acharya, S., and Gutmark, E. J., "Controlled Swirl-Stabilized Spray Combustor," AIAA Paper 97-0464, Jan. 1997.

[7]Stephens, J. R., Acharya, S., Gutmark, E. J., Allgood, D. C., and Murugappan, S., "Open Loop Control of a Swirl-Stabilized Liquid Fuel Diffusion Flame," AIAA Paper 98-0351, 1998.

[8]Stephens, J. R., "Swirl-Stabilized Spray Combustion with Active Control," M.S. Thesis, Louisiana State Univ., Baton Rouge, LA, 1998.

[9]Stephens, J. R., Acharya, S., and Gutmark, E. J., "Experimenal Study of Swirl-Stabilized Spray Combustion with Active Forcing," AIAA Paper 99-0330, 1999.

[10]Yu, K., Parr, T., Wilson, K., Schadow, K., and Gutmark, E., "Active Control of Liquid-Fueled Combustion Using Periodic Vortex-Droplet Interaction," *Twenty-Sixth (International) Symposium on Combustion*, Combustion Inst., Pittsburgh, PA, 1996.

[11]Chigier, A., and McReath, C. G., "Combustion of Droplets in Sprays," *Acta Astronautica*, Vol. 1, 1973.

[12]Hoinghaus, K. K., "Laser Techniques for the Quantitative Detection of Reactive Intermediates in Combustion Systems," *Progress in Energy and Combustion Science*, Vol. 20, 1994.

[13]Kelman, J. B., and Masri, A. R., "Simultaneous Imaging of Temperature and OH Number Density in Turbulent Diffusion Flames," *Combustion Science and Technology*, Vol. 122, 1997.

[14]Kelman, J. B., and Masri, A. R., "Quantitative Technique for Imaging Mixture Fraction, Temperature, and the Hydroxyl Radical in Turbulent Diffusion Flames," *Applied Optics*, Vol. 36, 1997.

[15]Stepowski, D., Cessou, A., and Goix, P., "Flame Stabilization and OH Fluorescence Mapping of the Near Field of a Spray Jet," *Combustion and Flame*, Vol. 99, 1994.

[16]Gutmark, E., Parr, T. P., Hanson-Parr, D. M., and Schadow, K. C., "Planar Imaging of Vortex Dynamics in Flames," *Journal of Heat Transfer*, Vol. 111, 1989.

[17]Allen, M. G., Hanson, R. K., "Digital Imaging of Species Concentrations Fields in Spray Flames," *Twenty-First (International) Symposium on Combustion*, Combustion Inst., Pittsburgh, PA, 1986.

[18]Allen, M. G., McManus, K. R., and Sonnenfroh, D. M., "PLIF Imaging Measurements in High-Pressure Spray Flame Combustion," 25th AIAA Plasmadynamics and Lasers Conf., 1994.

[19]Cessou, A., and Stepowski, D., "Planar Laser-Induced Fluorescence Measurement of [OH] in the Stabilization Stage of a Spray Jet Flame," *Combustion Science and Technology*, Vol. 118, 1996, p. 273.

[20]Hanson, R. K., Seitzman, J. M., and Paul, P. H., "Planar Laser-Fluorescence Imaging of Combustion Gases," *Applied Physics B*, Vol. 50, 1990.

[21]Grinstead, J. H., Laufer, G., Krauss, R. H., and McDaniel, J. C., "Calibration Source for OH Laser-Induced Fluorescence Density Measurements with Thermally Dissociated H2O in Atmospheric Air," *Applied Optics*, Vol. 33, 1994.

[22]Hoinghaus, K. K., Koczar, P., and Just, T. H., "Absolute Concentration Measurements of OH in Low-Pressure Hydrogen–Oxygen, Methane–Oxygen, and Acetylene—Oxygen Flames," *Twenty-First (International) Symposium on Combustion*, Combustion Inst., Pittsburgh, PA, 1986.